Journal of Computational Physics **174,** 649–668 (2001)
doi:10.1006/jcph.2001.6929, available online at http://www.idealibrary.com on IDEAL®

A Finite Difference Scheme Solving the Boltzmann–Poisson System for Semiconductor Devices

A. Majorana and R. M. Pidatella

Dipartimento di Matematica e Informatica, University of Catania, Viale A. Doria 6, I-95125 Catania, Italy
E-mail: majorana@dmi.unict.it, rosa@dmi.unict.it

Received September 28, 2000; revised June 1, 2001

The Boltzmann equation describing electron flow in semiconductor devices is considered. The collision operator models the scattering processes between free electrons and phonons in thermal equilibrium. The doping profile and the self-consistent electric field are related by the Poisson equation. The coupled system is solved by using a simple numerical scheme based on finite differences. Hydrodynamical variables are obtained by integrating the distribution function. Numerical results are shown for a one-dimensional $n^+ - n - n^+$ silicon diode. © 2001 Elsevier Science

Key Words: Boltzmann equation; difference schemes; semiconductors.

1. INTRODUCTION

The Boltzmann transport equation (BTE) describes electron transport in semiconductor devices. Solving it numerically is not an easy task, because the BTE is an integro–differential equation with six dimensions in the phase space and one in time. Actually, one of the most popular methods of modeling charge transport in such devices is the Monte Carlo method [4, 6, 10]. However, resolution of strong transients and an accurate description of the tail of the distribution function require an intractable number of particles to obtain good results. Moreover, it is also difficult to examine unsteady systems with Monte Carlo methods.

An alternative approach to the Monte Carlo method was proposed by Fatemi and Odeh [5]. They analyzed the exact BTE and developed a finite-difference scheme for solving the Boltzmann–Poisson system. Their interesting paper shows that a finite-difference scheme for solving this system is viable. This is possible also because the collision operator is simpler than the classical Boltzmann operator for perfect rarefied gas [3], where the five-dimensional manifold of the integrals suggests stochastic algorithms.

0021-9991/01 $35.00

In this paper we follow the main idea of [5], but a new numerical algorithm is proposed. In order to make clear the difference between the two schemes, we consider it useful to recall briefly some features of the Fatemi and Odeh [5] scheme. They used a spherical coordinate system for the wave-vector $\mathbf{k}$ and an upwind scheme to discretize the differential terms in the BTE. The spherical coordinates simplify the treatment of the collision operator but introduce a singularity in the free streaming operator. Since the transformed BTE is not defined at $\mathbf{k} = 0$, in order to avoid overflow in the numerical calculations a small neighborhood of the origin is removed from the $\mathbf{k}$ domain. This requires an additional non-physical boundary condition on the surface of this small region. In any case, when spherical coordinates are used, the origin of the Cartesian system is mapped into a rectangle and a new boundary condition is required. Moreover, in order to have a bounded $\mathbf{k}$ domain, a parameter k_{max} is suitably set and only the region $|\mathbf{k}| \leq k_{max}$ is considered. This new boundary requires again an additional condition, which must take into account the behavior of the distribution function for large values of $|\mathbf{k}|$ and the mass conservation law. Fatemi and Odeh [5] achieved this by also defining a modified collision operator directly in the discretized equations. Another small modification was performed on the collision operator of the BTE since it contains the Dirac distribution. In order to regularize this operator, a smooth function was used to replace the δ function. Consequently, the integral operator becomes compact and the mathematical and numerical treatment is simpler. Trouble arises because of the use of a smooth continuous function having compact support instead of the δ function. In fact, a small compact support gives a good approximation of the δ function but requires many grid points to ensure a good numerical discretization. On the other hand, a large support gives a dual situation. Therefore a careful but not trivial compromise was needed.

We develop a new scheme still based on spherical coordinates for the wave vector and finite differences to discretize partial and integral operators. The use of a new unknown, instead of the distribution function, allows us to automatically eliminate the singularity in the free streaming operator and to give the exact boundary condition corresponding to the origin of the $\mathbf{k}$ space.

We use a different approach for the treatment of the spatial coordinate $\mathbf{x}$ and the wave-vector $\mathbf{k}$. In fact we use the box method to discretize the BTE in the $\mathbf{k}$ space, and we use the upwind method in the $\mathbf{x}$ space. This choice arises from physical considerations and will be clearly explained later.

Before performing the numerical discretization, we introduce an upper bound for $|\mathbf{k}|$ in the kernel of the collision operator of the exact BTE. This modification still guarantees mass conservation. Moreover, we keep the Dirac distribution inside the collision operator.

The plan of the paper is as follows. In Section 2 we describe the main features of the model equations. The energy band structure is modeled assuming the Kane model instead of the parabolic band approximation used by Fatemi and Odeh [5]. In Section 3 the dimensionless equations are derived. In Section 4 we describe our numerical scheme. Finally, in Section 5 we show the results of a test problem and in Section 6 draw conclusions.

2. BASIC EQUATIONS

We consider an electron gas, which interacts with a bath of phonons assumed to be in thermal equilibrium. In this case the Boltzmann equation is [6, 9]

$$\frac{\partial f}{\partial t} + \frac{1}{\hbar}\nabla_{\mathbf{k}}\varepsilon \cdot \nabla_{\mathbf{x}} f - \frac{\mathfrak{e}}{\hbar}\mathbf{E} \cdot \nabla_{\mathbf{k}} f = Q(f). \tag{1}$$

The unknown f is the electron distribution function, which depends on time t, space coordinates x, and wave-vector k. The parameters $\hbar$ and $\mathfrak{e}$ are the Planck constant divided by 2π and the positive electric charge, respectively. The symbols ∇_{x} and ∇_{k} stand for the gradient with respect to the variables x and k, respectively. The particle energy ε is an assigned nonnegative continuous function. If the Kane model is assumed, then

$$\varepsilon(\mathsf{k}) = \frac{1}{1+\sqrt{1+2\frac{\tilde{\alpha}}{m^*}\hbar^2|\mathsf{k}|^2}}\frac{\hbar^2}{m^*}|\mathsf{k}|^2, \tag{2}$$

where m^* is the effective mass and $\tilde{\alpha}$ is the nonparabolicity factor. The widely used parabolic approximation is obtained from Eq. (2) by setting $\tilde{\alpha} = 0$. We adopt Eq. (2) because it gives a more realistic description of the electron band structure than the parabolic approximation.

In Eq. (1) the electric field E satisfies the Poisson equation

$$\Delta V = \frac{\mathfrak{e}}{\epsilon}[n(t,\mathsf{x}) - N_D(\mathsf{x})], \tag{3}$$

$$\mathsf{E} = -\nabla_{\mathsf{x}} V, \tag{4}$$

where ϵ is the permittivity, $n(t,\mathsf{x}) = \int_{\Re^3} f(t,\mathsf{x},\mathsf{k})\,d\mathsf{k}$ is the electron density, $N_D(\mathsf{x})$ is the doping, and V is the electric potential. Equations (1), (3), and (4) give the Boltzmann–Poisson system.

We follow a semiclassical approach for the collision term $Q(f)$, so that, in the low-density regime, it is

$$Q(f)(t,\mathsf{x},\mathsf{k}) = \int_{\mathbb{R}^3}[S(\mathsf{k}',\mathsf{k})f(t,\mathsf{x},\mathsf{k}') - S(\mathsf{k},\mathsf{k}')f(t,\mathsf{x},\mathsf{k})]\,d\mathsf{k}'. \tag{5}$$

The kernel S, which takes into account the scattering processes between electrons and phonons, is defined by

$$\begin{aligned} S(\mathsf{k},\mathsf{k}') = {} & K_0(\mathsf{k},\mathsf{k}')\delta(\varepsilon(\mathsf{k}') - \varepsilon(\mathsf{k})) + K(\mathsf{k},\mathsf{k}') \\ & \times[(\mathsf{n}_q+1)\delta(\varepsilon(\mathsf{k}') - \varepsilon(\mathsf{k}) + \hbar\omega) + \mathsf{n}_q\delta(\varepsilon(\mathsf{k}') - \varepsilon(\mathsf{k}) - \hbar\omega)]. \end{aligned} \tag{6}$$

The constant n_q is the occupation number of phonons and is given by

$$\mathsf{n}_q = \left[\exp\left(\frac{\hbar\omega}{k_B T_L}\right) - 1\right]^{-1},$$

where ω is the constant phonon frequency, k_B is the Boltzmann constant, and T_L is the lattice temperature. The symbol δ indicates the usual Dirac distribution. This is composed with the function $\varepsilon(\mathsf{k})$. The mathematical meaning of the new distribution function $\delta(\varepsilon(\mathsf{k}') - \varepsilon(\mathsf{k}) \pm \hbar\omega)$ is analyzed in [8].

The domain of the wave-vector is the $\mathbb{R}^3$ space. In order to eliminate this difficulty in the numerical calculations, one usually replaces $\mathbb{R}^3$ with a bounded domain. Fix a positive integer $\bar{N}$, and the new domain of the wave-vector is

$$D = \{\mathsf{k} \in \mathbb{R}^3 : \varepsilon(\mathsf{k}) \le \bar{N}\hbar\omega\}.$$

Following [7] we modify $Q(f)$ by multiplying the kernels—K_0 and K—by the step function

$$C(\varepsilon(\mathsf{k}), \varepsilon(\mathsf{k}')) = \begin{cases} 1 & \text{if } max\{\varepsilon, \varepsilon'\} < \bar{N}\hbar\omega \\ 0 & \text{otherwise.} \end{cases} \tag{7}$$

It is worthwhile to point out that it is possible, by using standard techniques, to prove that

$$\int_D Q(f)(t, \mathsf{x}, \mathsf{k})\, d\mathsf{k} = 0,$$

for every admissible f. This implies the mass conservation, assuming the boundary condition

$$f(t, \mathsf{x}, \mathsf{k}) = 0 \tag{8}$$

for every $(t, \mathsf{x}, \mathsf{k})$ such that $\varepsilon(\mathsf{k}) = \bar{N}\hbar\omega$.

The cut in the kernels means physically that an electron has zero probability of colliding in the following two cases:

- The electron, before the collision, has an energy less than $\bar{N}\hbar\omega$, but after has an energy equal to or greater than $\bar{N}\hbar\omega$.
- The electron, before the collision, has an energy greater than or equal to $\bar{N}\hbar w$.

This means that the number of all the electrons having energy less than $\bar{N}\hbar w$ does not change as an effect of collisions. The boundary condition Eq. (8) guarantees that the energy of a particle cannot exceed the threshold $\bar{N}\hbar\omega$ due to the electric field.

3. DIMENSIONLESS EQUATIONS

It is useful to introduce dimensionless equations. Now we use the coordinate transformation

$$\mathsf{k} = \sqrt{2}\frac{\sqrt{m^* k_B T_L}}{\hbar}\sqrt{w}\sqrt{1 + \alpha_K w}(\sqrt{1-\mu^2}\cos\phi,\ \sqrt{1-\mu^2}\sin\phi,\ \mu), \tag{9}$$

where $\alpha_K = k_B T_L \tilde{\alpha}$ and w is a dimensionless energy.

Equation (9) is equivalent to the spherical coordinate transformation when the parabolic band approximation is used. The main advantage of the new coordinates is the easy treatment of the δ function. In fact, it is simple to check that

$$\varepsilon = k_B T_L w,$$

so that the integrals with respect to w in the collision operator can be solved exactly by using the properties of the δ function.

The Jacobian of the transformation $\mathsf{k} \to (w, \phi, \mu)$ is

$$\frac{1}{2}\left(\frac{2m^* k_B T_L}{\hbar^2}\right)^{3/2}\sqrt{w(1+\alpha_K w)}(1 + 2\alpha_K w).$$

Let K_* be a dimensional constant parameter of the *same order* as the kernel K. Now, we define dimensionless quantities. In order to simplify the notation in the rest of the paper, here we put a tilde over the dimensional variables. Let

$$\alpha = \frac{\hbar\omega}{k_B T_L}, \qquad a = \frac{n_q + 1}{n_q} = e^{\alpha},$$

$$\tilde{K}(\mathsf{k}, \mathsf{k}') = K_* K(\boldsymbol{\xi}, \boldsymbol{\xi}'), \qquad \tilde{K}_0(\mathsf{k}, \mathsf{k}') = K_* n_q K_0(\boldsymbol{\xi}, \boldsymbol{\xi}'),$$

$$t_* = \left[4\sqrt{2}\pi \frac{m^* \sqrt{m_*}}{\hbar^3} \sqrt{k_B T_L}\, n_q K_*\right]^{-1}, \qquad l_* = \sqrt{\frac{k_B T_L}{m^*}}\, t_*,$$

$$\tilde{t} = t_*\, t, \qquad \tilde{\mathbf{x}} = \sqrt{2} l_* \mathbf{x},$$

$$\tilde{N}_D(\tilde{\mathbf{x}}) = \left(\frac{\sqrt{2m^* k_B T_L}}{\hbar}\right)^3 N_D(\mathbf{x}), \qquad c_p = \frac{2\sqrt{2}}{\epsilon} \mathfrak{e}^2 l_*^2 \frac{m^* \sqrt{m^*}}{\hbar^3} \sqrt{k_B T_L},$$

$$\mathsf{E}(t, \mathbf{x}) = \sqrt{2} \frac{k_B T_L}{\mathfrak{e} l_*} (E_1(\tilde{t}, \tilde{\mathbf{x}}), E_2(\tilde{t}, \tilde{\mathbf{x}}), E(\tilde{t}, \tilde{\mathbf{x}})), \qquad V(t, \mathbf{x}) = 2 \frac{k_B T_L}{\mathfrak{e}} \Psi(\tilde{t}, \tilde{\mathbf{x}}),$$

where $\boldsymbol{\xi} = (w, \phi, \mu)$. Here z is the spatial coordinate and t is the dimensionless time.

In the following we will see that an appropriate choice of K_* makes t_* and l_* of the same order of magnitude as the characteristic time scale and length of the semiconductor, respectively.

In terms of the new variables, the unknown f is denoted by F. Since we are looking for a solution of the BTE, which depends only on one spatial coordinate, we simply write $F(t, z, w, \mu)$. It is obvious that the electric potential depends only on t and z. The angular coordinate ϕ disappears, due to the symmetry of the problem.

Let

$$\Phi(t, z, w, \mu) = s(w) F(t, z, w, \mu). \tag{10}$$

The function Φ will be the new unknown. Since the function $s(w)$ is proportional to the Jacobian of the coordinate transformation, we can evaluate moments of the distribution function, as density or momentum, using Φ directly. In fact, as an example, the density of the gas is given, apart from a dimensional factor, by

$$\frac{1}{2} \int_0^{2\pi} d\phi \int_0^{+\infty} dw \int_{-1}^{1} d\mu \Phi(t, z, w, \mu).$$

We are interested in solving the Boltzmann–Poisson system in the case of a silicon device. The appropriate kernels $\tilde{K}$ and $\tilde{K}_0$ are then constant (see Appendix A for the numerical data). Now, we can choose K_* such that

$$\tilde{K} = 1 \quad \text{and} \quad \tilde{K}_0 = \beta \simeq 5.986.$$

Then $t_* \simeq 3.6$ ps and $l_* \simeq 0.43\,\mu$m.

It follows that the collisional operator becomes

$$Q(f)(\mathsf{k}) = \frac{1}{t_*} \left\{ \frac{1}{2} \int_{-1}^{1} [\beta \Phi(t, z, w, \mu') + a \Phi(t, z, w + \alpha, \mu') + \Phi(t, z, w - \alpha, \mu')]\, d\mu' \right.$$
$$\left. - \frac{1}{s(w)} [\beta s(w) + a s(w - \alpha) + s(w + \alpha)] \Phi(t, z, w, \mu) \right\}; \tag{11}$$

the forcing term is

$$-\frac{e}{\hbar}\mathsf{E}\cdot\nabla_{\mathsf{k}} f = -\frac{E}{t_*}\left[\frac{2\mu\sqrt{w(1+\alpha_K w)}}{(1+2\alpha_K w)}\frac{\partial}{\partial w}\left(\frac{\Phi}{s(w)}\right)+\frac{(1-\mu^2)}{w(1+\alpha_K w)(1+2\alpha_K w)}\frac{\partial\Phi}{\partial\mu}\right];$$

and, finally, the convective term is

$$\frac{1}{\hbar}\frac{\partial\varepsilon}{\partial k_3}\cdot\frac{\partial f}{\partial x_3}=\frac{1}{t_*}\frac{\mu}{(1+2\alpha_K w)^2}\frac{\partial\Phi}{\partial z},$$

where k_3 is the third component of k, and x_3 is the third component of x. The Poisson equation is now

$$\frac{\partial^2\Psi}{\partial z^2}=-c_p\left[N_D(z)-\pi\int_0^{+\infty}dw\int_{-1}^{1}d\mu\ \Phi(t,z,w,\mu)\right].$$

The domains of the variables are

$$z\in[0,L],\quad w\in[0,w_{max}],\quad \mu\in[-1,1],$$

where L is the dimensionless length of the device and $w_{max}=\bar{N}\hbar\omega$ is the maximum value of the energy, which is adjusted in the numerical experiments such that

$$F(t,z,w,\mu)\simeq 0\quad \text{for } w\geq w_{max},\quad \text{for every } t,z,\mu.$$

Of course we modify Eq. (11) taking into account the cut described previously.

4. NUMERICAL SCHEME

We perform, as the first step, the discretization only in w and μ. Let Δw and $\Delta\mu$ denote the constant step sizes. The presence of the δ function requires us to assume that $\alpha/\Delta w$ is an integer in order to treat the shifted terms $\Phi(t,z,w\pm\alpha,\mu)$ correctly. The grid points in the $w-\mu$ space are

$$w_i=i\cdot\Delta w,\quad \mu_j=-1+j\cdot\Delta\mu,\quad i,j=0,1,2,\ldots.$$

For each interior point (w_i,μ_j) we consider the rectangle $R_{ij}=[w_{i-1},w_{i+1}]\times[\mu_{j-1},\mu_{j+1}]$. Now, we multiply both sides of the BTE by $s(w)$ and integrate with respect to w and μ on R_{ij}. An easy computation shows that the following equation is obtained.

$$\begin{aligned}
&\frac{\partial}{\partial t}\iint_{R_{ij}}\Phi(t,z,w,\mu)\,dw\,d\mu+\iint_{R_{ij}}\frac{\sqrt{w(1+\alpha_K w)}}{(1+2\alpha_K w)}\mu\frac{\partial\Phi}{\partial z}\,dw\,d\mu\\
&\quad -E(t,z)\left\{\int_{\mu_{j-1}}^{\mu_{j+1}}d\mu\left[2\mu\frac{\sqrt{w(1+\alpha_K w)}}{(1+2\alpha_K w)}\Phi(t,z,w,\mu)\right]_{w_{i-1}}^{w_{i+1}}\right.\\
&\quad \left.+\int_{w_{i-1}}^{w_{i+1}}dw\left[\frac{1-\mu^2}{\sqrt{w(1+\alpha_K w)}}\Phi(t,z,w,\mu)\right]_{\mu_{j-1}}^{\mu_{j+1}}\right\}\\
&=\Delta\mu\int_{w_{i-1}}^{w_{i+1}}dw\int_{-1}^{1}d\mu[\beta\Phi(t,z,w,\mu)+a\Phi(t,z,w+\alpha,\mu)+\Phi(t,z,w-\alpha,\mu)]s(w)\\
&\quad -\iint_{R_{ij}}[\beta s(w)+as(w-\alpha)+s(w+\alpha)]\Phi(t,z,w,\mu)\,dw\,d\mu. \qquad (12)
\end{aligned}$$

The cut in the collision operator simply implies that in Eq. (12) we must define $s(w) = 0$ if $w \notin (0, w_{max})$ and set $\Phi(t, z, w, \mu) = 0$ if $w \geq w_{max}$ for every (t, z, μ). We notice that integration by parts in the forcing term gives one-dimensional integrals. We remark that Eq. (12) contains only a term, which is singular for $w = 0$, but it is integrable.

This approach is usually called a box scheme. The integrals in Eq. (12) are numerically approximated by using quadrature formulas. For the first term in Eq. (12) one can simply use

$$\iint_{R_{ij}} \Phi(t, z, w, \mu)\, dw\, d\mu \simeq 4\Delta w \Delta \mu \Phi(t, z, w_i, \mu_j).$$

For the other integrals the Simpson rule is applied, except for the integral

$$\int_0^{2\Delta w} \left[\frac{1-\mu^2}{\sqrt{w(1+\alpha_K w)}} \Phi(t, z, w, \mu) \right]_{\mu_{j-1}}^{\mu_{j+1}} dw,$$

where a parabolic interpolation for the function $\Phi(t, z, w, \mu)/\sqrt{1+\alpha_K w}$ is used because of the singularity.

The values of Φ on the boundary of the $w - \mu$ domain are determined as follows. We have

$$\Phi(t, z, 0, \mu) = 0 \quad \text{for every } (t, z, \mu)$$

due to the definition of Φ (Eq. (10)), and

$$\Phi(t, z, w_{max}, \mu) = 0 \quad \text{for every } (t, z, \mu)$$

due to the boundary condition Eq. (8).

The values of Φ for $\mu = \pm 1$ are easily obtained by the relations

$$\Phi(t, z, w, 1) = \Phi(t, z, w, 1 - \Delta\mu)$$
$$\Phi(t, z, w, -1) = \Phi(t, z, w, -1 + \Delta\mu)$$

for every (t, z, w). We choose the same boundary conditions for the inflow and outflow of electrons as in [5]; i.e.,

$$\frac{\partial \Phi}{\partial z}(t, 0, w, \mu) = 0 \quad \text{if } \mu > 0, \quad \frac{\partial \Phi}{\partial z}(t, 1, w, \mu) = 0 \quad \text{if } \mu < 0,$$

for every t and w.

At this stage we have a large system of partial differential equations in (t, z). The nature of the BTE would make the previous system hyperbolic, but we do not prove it. So classical difference schemes for the advection equation can be applied. We use the upwind method, as in [5]. We remark that, for each (i, j), Eq. (12) gives an equation which contains nine partial derivatives with respect to z, due to the two-dimensional Simpson rule.

The ordinary differential equations obtained after the spatial discretization are solved using standard predictor–corrector schemes. Our numerical experiments suggest the use of high order (four or five) formulas. The initial condition for f is a local Maxwellian distribution (see Appendix A).

The Poisson equation is solved formally. The numerical scheme giving an approximation of the solution is described in Appendix B. It differs from the standard scheme because

in this way it is possible to use grid points not equally distributed. The solution of the Poisson equation is performed at each step of the predictor–corrector iteration, resembling a *frozen-in-time* electric field.

5. NUMERICAL RESULTS

We choose the $n^+ - n - n^+$ silicon diode as a test problem. The doping densities and the length of the regions are

$$N_D(z) = 5 \cdot 10^{17}\,\mathrm{cm}^{-3} \quad \text{for } 0 \le z \le 0.3\ (\mu\mathrm{m}) \quad \text{and} \quad 0.7 \le z \le 1\ (\mu\mathrm{m})$$
$$N_D(z) = 2 \cdot 10^{15}\ \mathrm{cm}^{-3} \quad \text{for } 0.3 \le z \le 0.7\ (\mu\mathrm{m}).$$

We used a $V_{bias} = 1V$ and the same constants as in [1].

For the discretization of the variables t, z, w, μ we used the following values. For z we have both equally and unequally spaced grid points. In the first case, a cell has a length of L/N_z, where $L = 1$ μm is the length of our device and N_z is the number of cells of the discretization. We used $N_z = 512$, 256, and 128. In the case of a grid not equally spaced we have $N_z = 180$ but distributed in this way: 15 cells for each interval [0, 0.25] and [0.75, 1], 40 cells for [0.25, 0.35] and [0.65, 0.75], and 70 cells for [0.35, 0.65].

For the discretization of w and μ we have $\Delta w = \alpha/4$ and $\Delta\mu = 1/15$. Finally, the number of time-steps per picosecond varies from 300 to 560 depending on the minimum value of the length of the cells.

We perform some numerical experiments to see the influence of the *length* of the junctions. The simplest case but the most unrealistic one is to use the step function. The second case

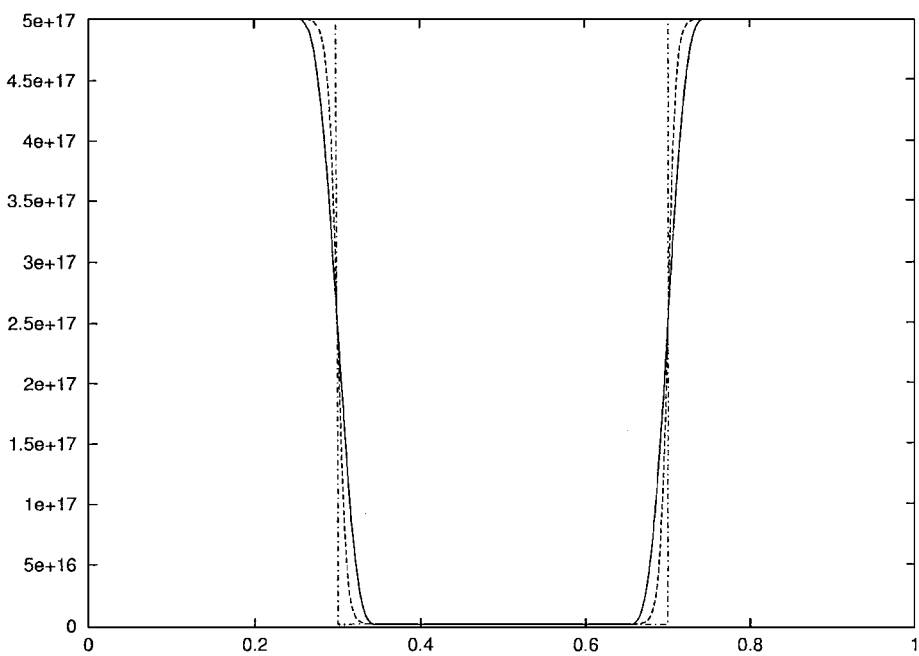

FIG. 1. Doping density profile for the three cases. Fatemi and Odeh [5]: continuous line; Anile *et al.* [2]: dashed line; step function: dot-dash line.

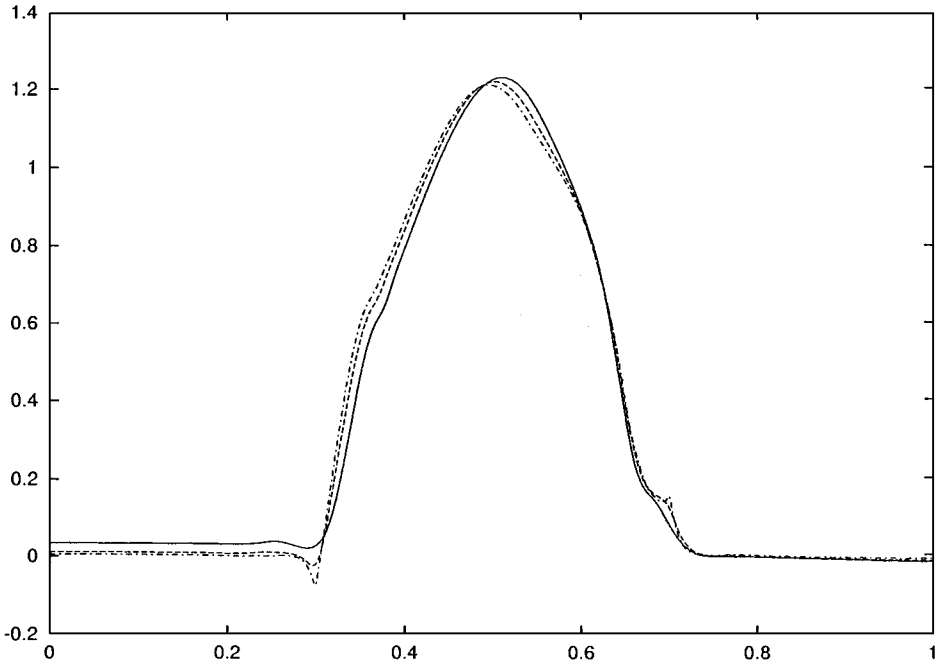

FIG. 2. Velocity for $t = 1$ ps, $N_z = 512$, and three doping profiles: Fatemi and Odeh [5]: continuous line; Anile *et al*. [2]: dashed line; step function: dot-dash line.

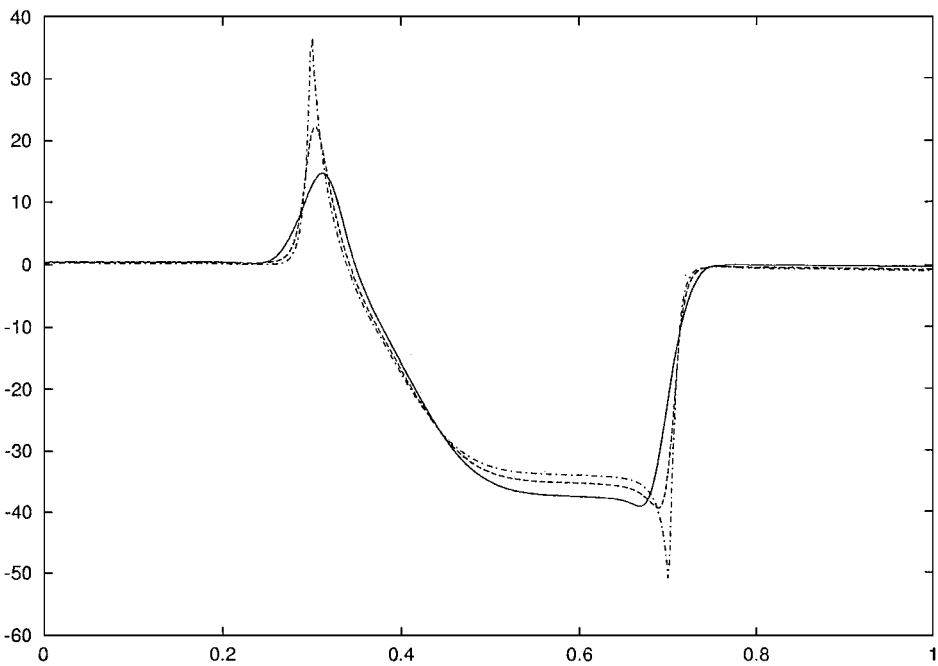

FIG. 3. Electric field for $t = 1$ ps, $N_z = 512$, and three doping profiles: Fatemi and Odeh [5]: continuous line; Anile *et al*. [2]: dashed line; step function: dot-dash line.

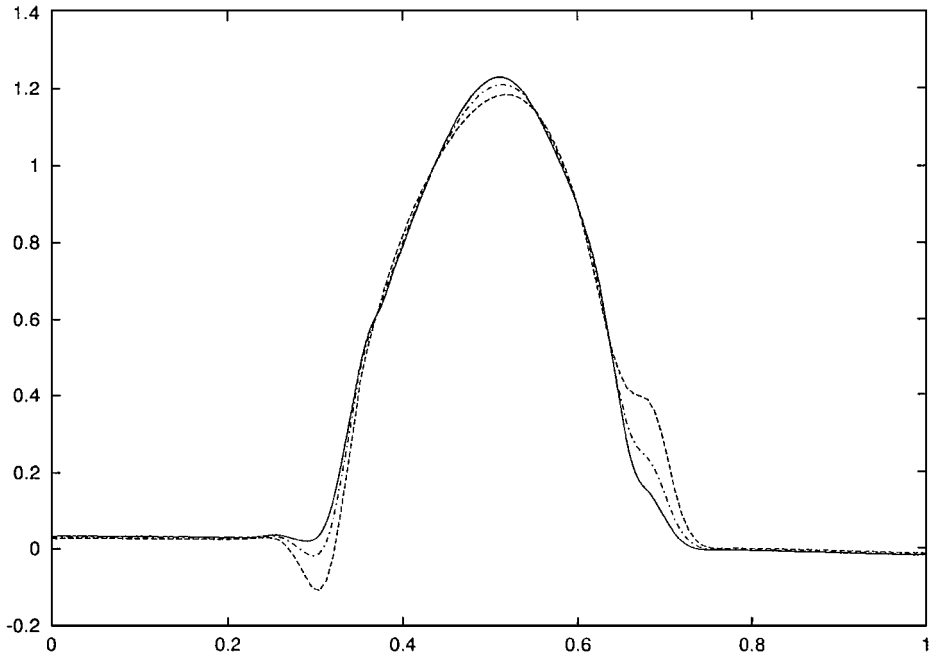

FIG. 4. Velocity for $t = 1$ ps and $N_z = 512$: continuous line; 256: dot-dash line; 128: dashed line.

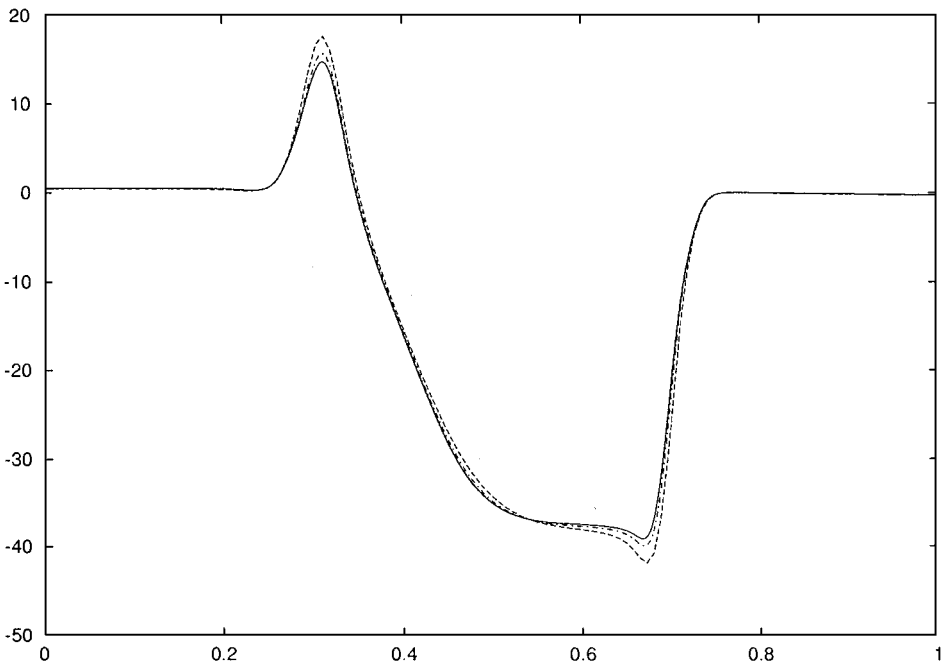

FIG. 5. Electric field for $t = 1$ ps and $N_z = 512$: continuous line; 256: dot-dash line; 128: dashed line.

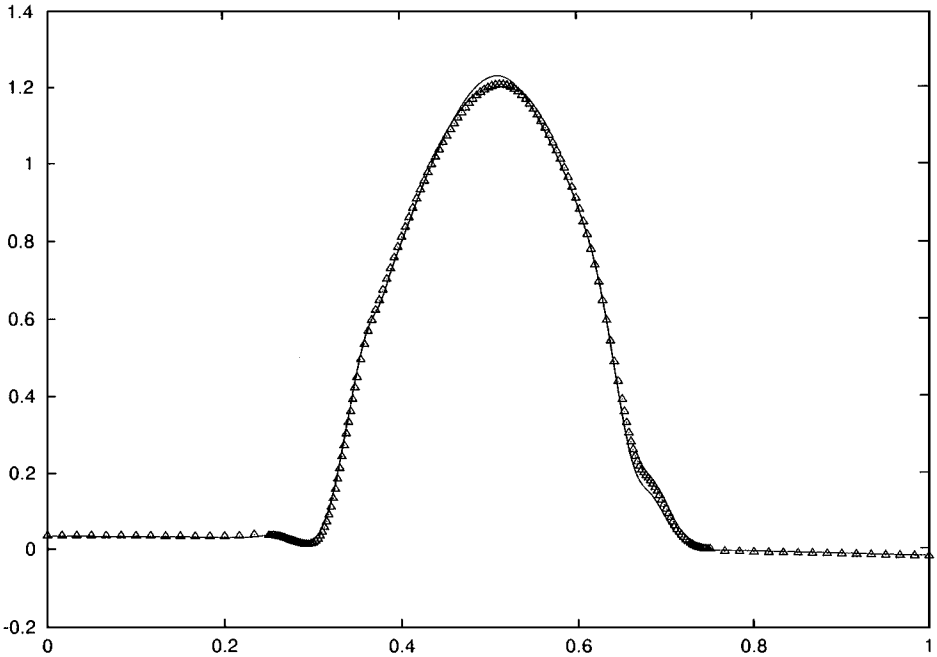

FIG. 6. Velocity for $t = 1$ ps and $N_z = 512$: continuous line; 180: triangles.

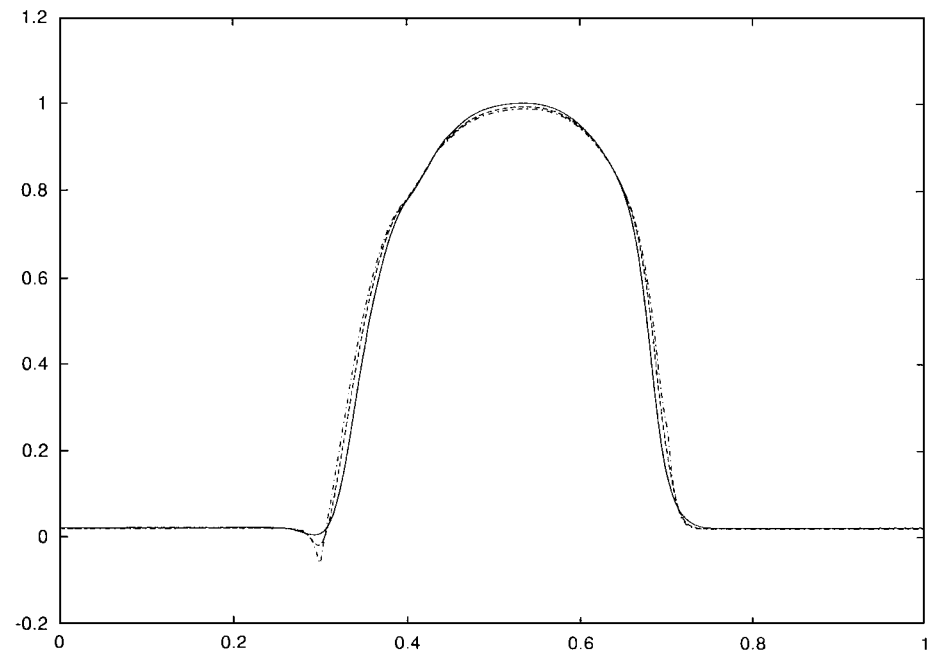

FIG. 7. Velocity for $t = 5$ ps, $N_z = 512$ for three doping profiles: Fatemi and Odeh [5]: continuous line; Anile *et al.*: dashed line; step function: dot-dash line.

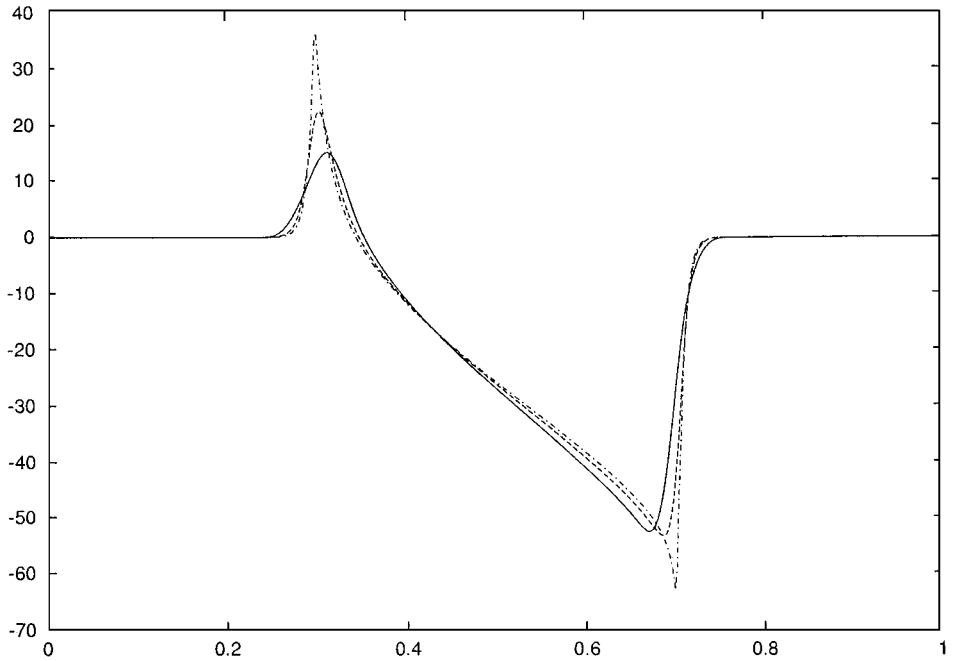

FIG. 8. Electric field for $t = 5$ ps and $N_z = 512$ for three doping profiles: Fatemi and Odeh [5]: continuous line; Anile *et al*.: dashed line; step function: dot-dash line.

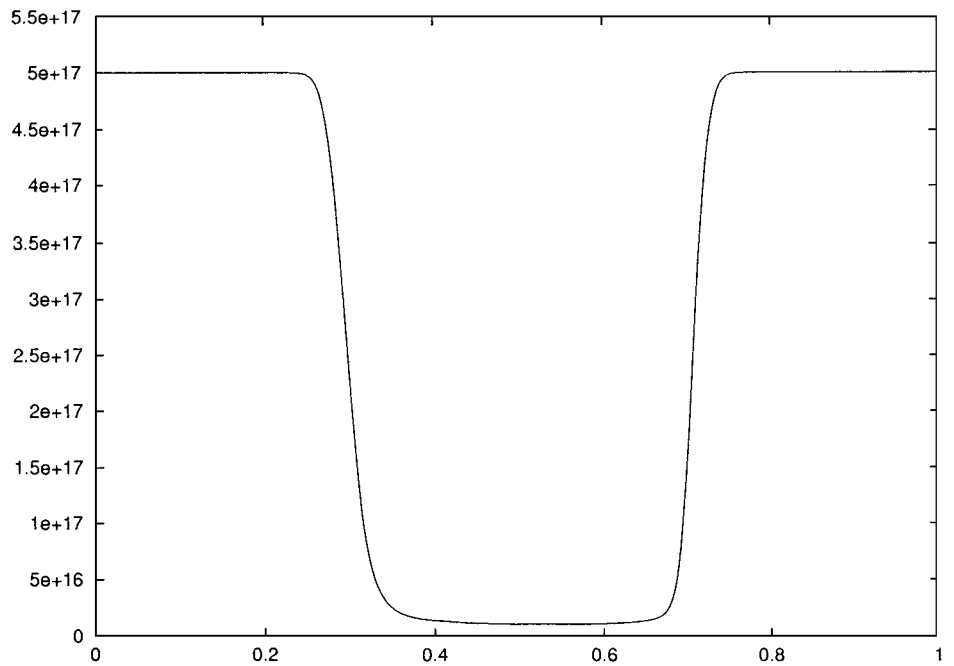

FIG. 9. Density for $t = 5$ ps and $N_z = 512$.

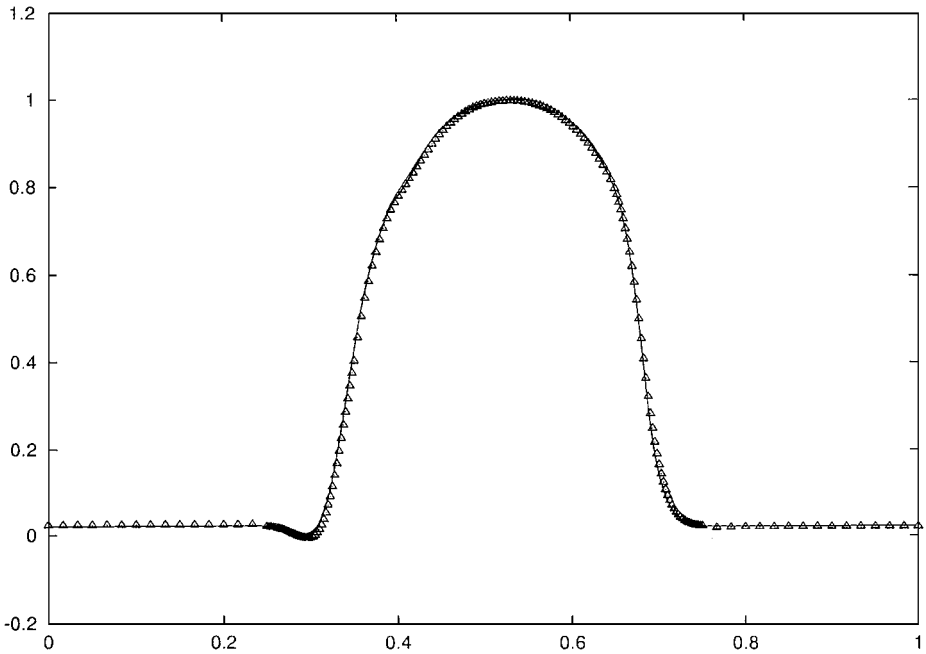

FIG. 10. Velocity for $t = 5$ ps and $N_z = 512$: continuous line; 180: triangles.

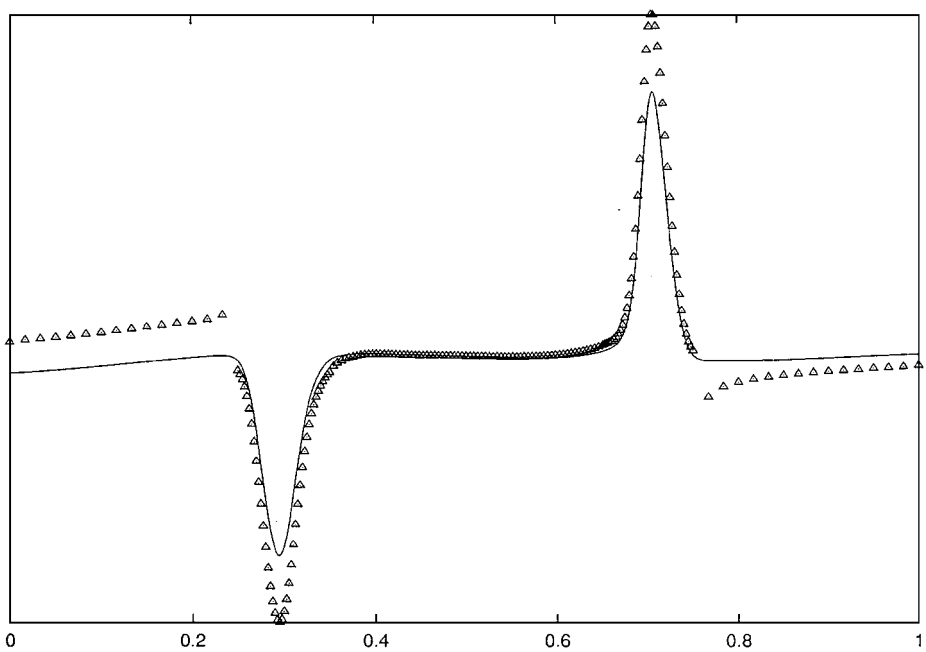

FIG. 11. Momentum for $t = 5$ ps and $N_z = 512$: continuous line; 180: triangles.

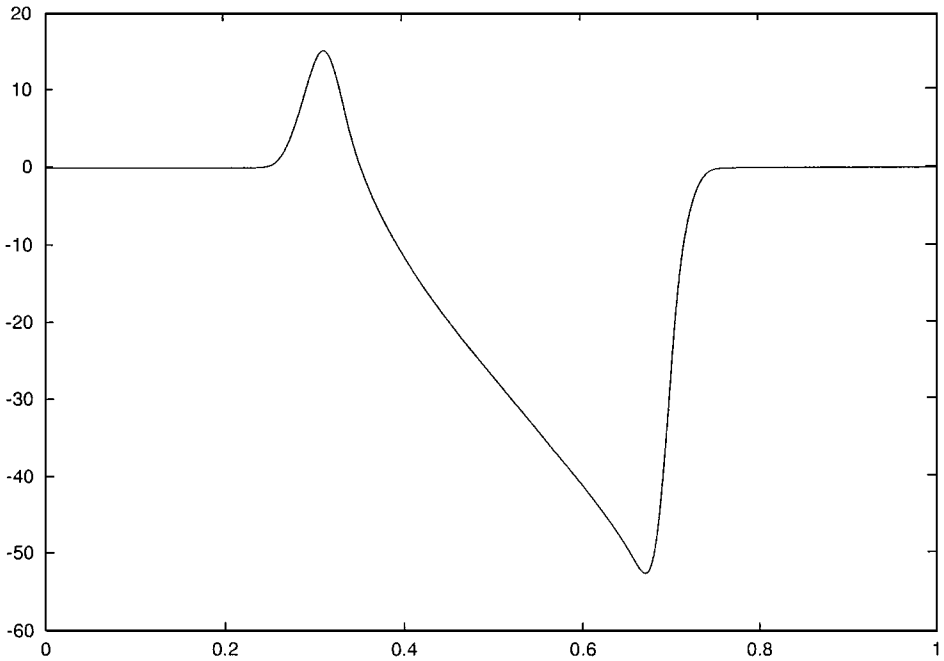

FIG. 12. Electric field for $t = 5$ ps and $N_z = 512$.

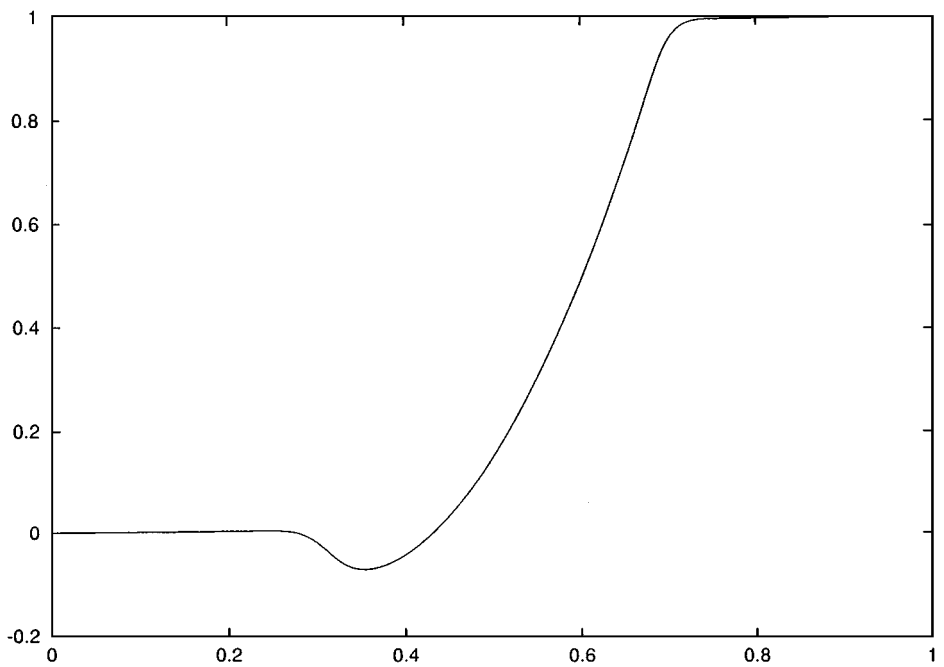

FIG. 13. Electric potential for $t = 5$ ps and $N_z = 512$.

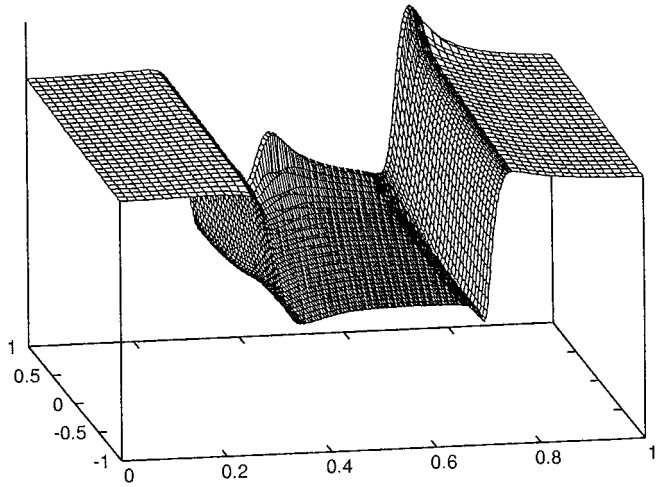

FIG. 14. Distribution function for $t = 5$ ps at $\epsilon = 2\ \hbar\omega$.

we considered is a doping profile regularized according to the function [2]

$$N_D(0) - d_0\left(\tanh\frac{z - z_1}{s} - \tanh\frac{z - z_2}{s}\right),$$

where $d_0 = [N_D(0) - N_D(0.5)]/2$, $z_1 = 0.3\ \mu$m, $z_2 = 0.7\ \mu$m, and the parameter $s = 0.01\ \mu$m. The third case is that of Fatemi and Odeh [5], where the profile is regularized with a seven-degree polynomial. Figure 1 shows three different doping profiles using step function, hyperbolic function, and piecewise polynomial.

The units used in the figures are the following: length in μm, velocity in 10^5 m s^{-1}, electric field in V m^{-1}, electric potential in kV, density in cm^{-3}, and energy in $\hbar\omega$. In Figs. 2 and 3 we see the effect of the three different doping profiles for velocity and

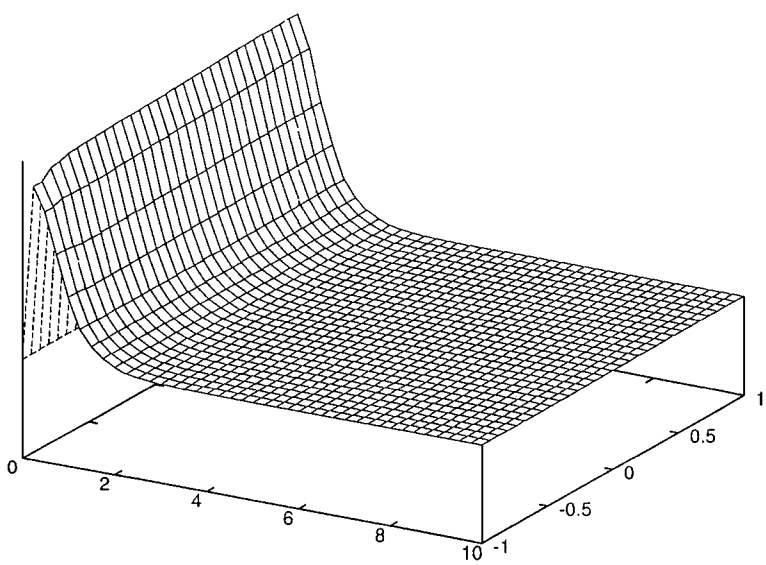

FIG. 15. Distribution function for $t = 5$ ps at $z = 0.2\ \mu$m.

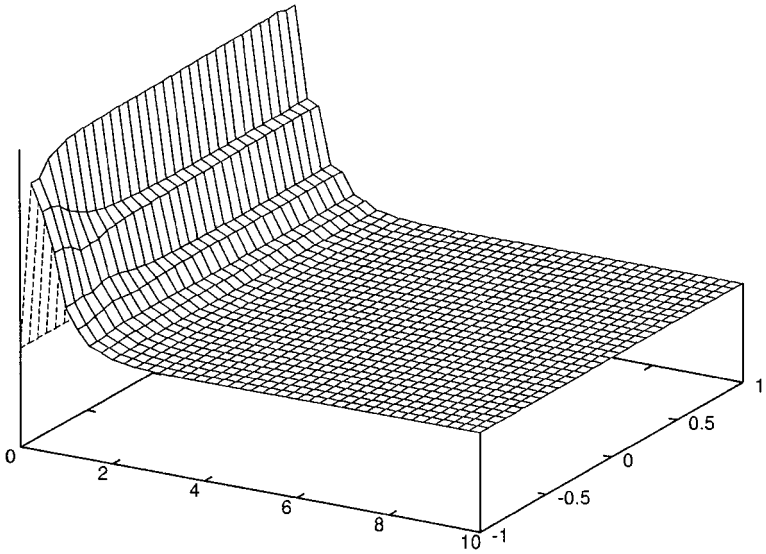

FIG. 16. Distribution function for $t = 5$ ps at $z = 0.3$ μm.

electric field in the transient (we chose $t = 1$ ps). We notice that the step function gives irregular profiles, while the other profiles give more regular results in the other cases. In Figs. 4 and 5 the influence of the number of cells is analyzed. We see that the nonphysical behavior near the first junction is numerical and it goes away with a finer discretization. Figure 6 suggests that it is possible to optimize the code using an irregular mesh with more points near the junctions but fewer points in the regular regions. Figures 7–17 refer to the numerical stationary case ($t = 5$ ps). Figures 7 and 8 show that the behavior is the same as in the transient, giving irregularities with the use of a step function. Figures 9–13 show density, velocity, momentum, electric field, and potential in the stationary case. In

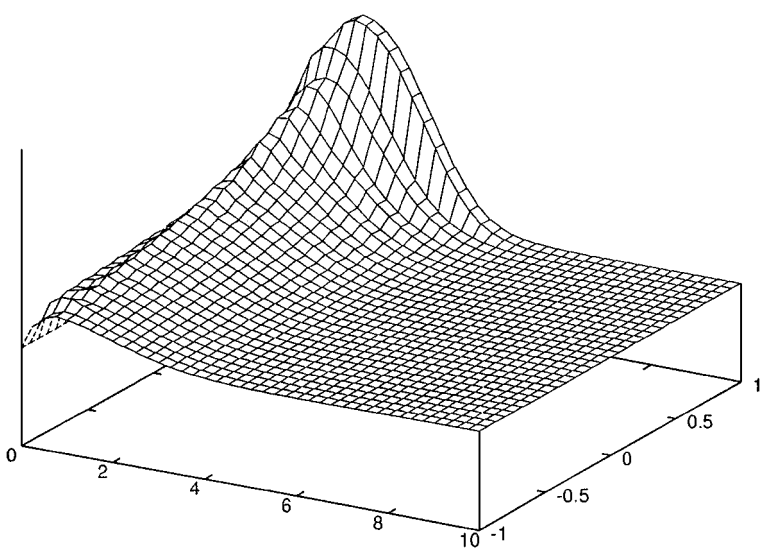

FIG. 17. Distribution function for $t = 5$ ps at $z = 0.5$ μm.

Figs. 10 and 11 we plot results with a regular ($N_z = 512$) and an irregular ($N_z = 180$) mesh, showing nearly no difference between the two discretizations. In the other cases, the two discretizations give the same results. We notice that the velocity, which is greater than the saturation velocity in the transient (Fig. 6), has a lower value in the stationary case (Fig. 10). Momentum is regular (Fig. 11), although there is a small residual error near the junctions.

To see the behavior of the distribution function Φ, we plot it for a fixed energy ($\varepsilon = 2\,\hbar\omega$) (Fig. 14) and for three fixed z: Fig. 15 at $z = 0.2\ \mu$m, Fig. 16 at $z = 0.3\ \mu$m, and Fig. 17 at $z = 0.5\ \mu$m. We notice that, in all the cases and even in the junctions, the function maintains a regular shape. The use of the box method allowed us to adopt high order formulas, like Simpson's rule, to solve integrals. This means that we can use very few points in w and μ. Moreover, we were able to obtain regular solutions even with nonsmooth profiles in doping, such as the step function.

6. CONCLUDING REMARKS

One advantage of the scheme used to solve the BTE is that it is possible to consider a collisional operator more complex than (5). We show some possible cases. In order to make our arguments clear, we recall that the finite-difference approximation to the BTE is achieved in two steps. The first concerns the k variables and consists in integrating Eq. (1), after a change of variables, over a small domain of k space (see Eq. (12)). In terms of dimensional variables these domains are

$$\Omega_{ij} = \{\mathsf{k} \in \mathbb{R}^3 : w_{i-1} \le w \le w_{i+1},\ \mu_{j-1} \le \mu \le \mu_{j+1},\ 0 \le \phi \le 2\pi\},$$

where w, μ, ϕ are related to k by Eq. (9). Using the original dimensional variables k, we obtain the equation

$$\int_{\Omega_{ij}} \left[\frac{\partial f}{\partial t} + \frac{1}{\hbar} \nabla_{\mathsf{k}} \varepsilon \cdot \nabla_{\mathsf{x}} f - \frac{\mathfrak{e}}{\hbar} \mathsf{E} \cdot \nabla_{\mathsf{k}} f \right] d\mathsf{k} = \int_{\Omega_{ij}} Q(f)\, d\mathsf{k}. \tag{13}$$

This equation, after the transformation (9), gives Eq. (12). Let us analyze the right-hand side of Eq. (13). If $\chi_{ij}(\mathsf{k})$ denotes the characteristic function of the set Ω_{ij}, then we have

$$\begin{aligned}
\int_{\Omega_{ij}} Q(f)(t,\mathsf{x},\mathsf{k})\, d\mathsf{k} &= \int_{\mathbb{R}^3} Q(f)(t,\mathsf{x},\mathsf{k}) \chi_{ij}(\mathsf{k})\, d\mathsf{k} \\
&= \int_{\mathbb{R}^3} \left[\int_{\mathbb{R}^3} S(\mathsf{k}',\mathsf{k})\, f(t,\mathsf{x},\mathsf{k}')\, d\mathsf{k}' \right] \chi_{ij}(\mathsf{k})\, d\mathsf{k} - \int_{\mathbb{R}^3} \left[\int_{\mathbb{R}^3} S(\mathsf{k},\mathsf{k}')\, f(t,\mathsf{x},\mathsf{k})\, d\mathsf{k}' \right] \chi_{ij}(\mathsf{k})\, d\mathsf{k} \\
&= \int_{\mathbb{R}^3} \left[\int_{\mathbb{R}^3} S(\mathsf{k}',\mathsf{k}) \chi_{ij}(\mathsf{k})\, d\mathsf{k} \right] f(t,\mathsf{x},\mathsf{k}')\, d\mathsf{k}' - \int_{\mathbb{R}^3} \left[\int_{\mathbb{R}^3} S(\mathsf{k},\mathsf{k}')\, d\mathsf{k}' \right] f(t,\mathsf{x},\mathsf{k}) \chi_{ij}(\mathsf{k})\, d\mathsf{k} \\
&= \int_{\mathbb{R}^3} \left[\int_{\Omega_{ij}} S(\mathsf{k}',\mathsf{k})\, d\mathsf{k} \right] f(t,\mathsf{x},\mathsf{k}')\, d\mathsf{k}' - \int_{\Omega_{ij}} \left[\int_{\mathbb{R}^3} S(\mathsf{k},\mathsf{k}')\, d\mathsf{k}' \right] f(t,\mathsf{x},\mathsf{k})\, d\mathsf{k}.
\end{aligned}$$

Now, it is clear that we can evaluate the integrals

$$\int_{\Omega_{ij}} S(\mathsf{k},\mathsf{k}')\, d\mathsf{k}' \quad \text{and} \quad \int_{\mathbb{R}^3} S(\mathsf{k},\mathsf{k}')\, d\mathsf{k}', \tag{14}$$

independently of the unknown f. Of course, we must calculate the integrals in Eq. (14) only for values of k which correspond to grid points in (w, μ)-space. Therefore, scattering kernels more complex than (6) can be considered. For example, the transition probability of an electron from state k to state k' can include all the possible phonon states; i.e., the phonon frequency does not have to be constant. Integrals (14) can be approximated numerically, but in this case, it is necessary to evaluate the second integral, considering the whole space $\mathbb{R}^3$ as the union of Ω_{ij} domains (i and j odd), and then using the same formulas as in the first integral (14). This guarantees that the mass conservation holds.

Another problem concerns the possibility of including the Pauli exclusion principle in the collision operator. This is important for high-density electron gas. In the case of constant phonon frequency, the inclusion of a $(1 - f)$ term into $Q(f)$ gives a nonlinear collisional integral instead of Eq. (11), but the numerical scheme is able to take this new situation into account. It is simple to imagine the new form of Eq. (12). The possibility of also including complex scattering kernels is not obvious, and it is evident that the arguments given above in this section are not applicable.

It is also reasonable that it is not possible to include the full collisional operator describing the electron–electron interaction, because of the five-dimensional integrals. The treatment of this operator, in fact, usually requires Monte Carlo algorithms instead of finite difference formulas. A possible way to overcome this difficulty is to consider a BGK collisional operator (relaxation model) (see, e.g., [3]) to describe carrier–carrier scattering. Toward this aim it is necessary to choose a suitable relaxation time (usually depending on the electron energy).

The second step of the finite-difference approximation concerns the x-variable. This point is important for the simulation of 2D devices. The dimension of the problem increases by one, since we need only an additional spatial coordinate. Our experiments for a 1D diode indicate that a reasonable small number of grid points in (w, μ)-space are needed. Then, simulations of 2D problems are related to a realistic spatial grid that is not too fine.

We want to point out that this work is a first attempt at a robust and efficient code to solve the BTE. Our future work will consider two different issues, again in the framework of 1D simulations. One is that of improving the numerical accuracy, for example, by using a higher order scheme for the discretization of spatial derivatives. Another issue is the improvement of the grid discretization by using, for example, adaptive mesh refinement algorithms. We think these improvements are necessary before attempting 2D device simulations.

APPENDIX A

Initial Conditions

The initial value of Φ is a locally Maxwellian distribution at the temperature T_L,

$$\Phi(0, z, w, \mu) = s(w) N_D(z) e^{-w} \left[2\pi \int_0^{+\infty} s(w) e^{-w}\, dw \right]^{-1},$$

so that the initial value for the density is equal to doping.

Numerical Values

We used the quantities

$$\begin{aligned}
\hbar w &= 0.063 \text{ eV} & T_L &= 300 \text{ K}^\circ \\
\tilde{\alpha} &= 0.5 \text{ (eV)}^{-1} & \rho_0 &= 2330 \text{ Kg m}^{-3} \\
\epsilon_0 &= 8.85419 \cdot 10^{-12} \text{ F m}^{-1} & \epsilon &= 11.7 \cdot \epsilon_0 \\
m_* &= 0.32 \cdot m_0 & u_l &= 9040 \text{ ms}^{-1} \\
D_t k &= 11.4 \cdot 10^{10} \text{ eV m}^{-1} & E_{ac} &= 9 \text{ eV} \\
K &= D_t k^2/(8\pi^2 \rho_0 \omega) & K_0 &= k_B T_L E_{ac}^2/\left(4\pi\hbar u_l^2 \rho_0\right) \\
\alpha &= 2.43694 & a &= 11.438 \\
\beta &= 5.986 & K_* &= 1.89405 \cdot 10^{-35}, \\
n_q &= 0.0958036 &&
\end{aligned}$$

where m_0 is the electron mass, ρ_0 is the crystal density, $D_t k$ is the optical coupling constant, u_l is the sound velocity, and E_{ac} is the deformation potential.

APPENDIX B

Poisson Equation

The exact solution of the Poisson equation is easily obtained by solving

$$\begin{cases} y'' = g(x) \\ y(a) = y_a, \quad y(b) = y_b. \end{cases}$$

We obtain

$$y(x) = y_a + \frac{x-a}{b-a}\left[y_b - y_a - \int_a^b (b-t)g(t)\,dt\right] + \int_a^x (x-t)g(t)\,dt$$

and

$$y'(x) = \frac{1}{b-a}\left[y_b - y_a - \int_a^b (b-t)g(t)\,dt\right] + \int_a^x g(t)\,dt.$$

The integrals are approximated using the trapezoidal rule.

ACKNOWLEDGMENTS

We acknowledge partial support from the Italian Consiglio Nazionale delle Ricerche (Prog. N. 97.04709.PS01), MURST (Prog. Mathematical Problems of Kinetic Theories 1998), and the TMR Network (asymptotic methods in kinetic theory, Grant, N. ERB-FMBX-CT97–0157).

REFERENCES

1. A. M. Anile, N. Nikiforakis, and R. M. Pidatella, Assessment of a high resolution centered scheme for the solution of hydrodynamical semiconductor equations, *SIAM J. Sci. Comput.* **22**(5), 1533 (2000).
2. A. M. Anile, V. Romano, and G. Russo, Extended hydrodynamical model of carrier transport in semiconductors, *SIAM J. Appl. Math.* **61**(1), 74 (2000).

3. C. Cercignani, *The Boltzmann Equation and Its Application* (Springer-Verlag, Berlin/New York, 1988).
4. M. V. Fischetti and S. E. Laux, Monte Carlo analysis of electron transport in small semiconductor devices including band-structure and space-charge effects, *Phys. Rev. B* **38**(14), 9721 (1988).
5. E. Fatemi and F. Odeh, Upwind finite difference solution of Boltzmann equation applied to electron transport in semiconductor devices, *J. Comput. Phys.* **108**, 209 (1993).
6. C. Jacoboni and P. Lugli, *The Monte Carlo Method for Semiconductor Device Simulation* (Springer-Verlag, New York/Berlin, 1989).
7. A. Majorana and C. Drago, A boundary value problem for a kinetic model describing electron flow in a semiconductor, *Math. Meth. Appl. Sci.* **23**, 735 (2000).
8. A. Majorana and A. Marano, Space homogeneous solutions to the Cauchy problem for semiconductor Boltzmann equations, *SIAM J. Math. Anal.* **28**, 1294 (1997).
9. P. A. Markowich, C. Ringhofer, and C. Schmeiser, *Semiconductor Equations* (Springer-Verlag, New York/Berlin, 1990).
10. K. Tomizawa, *Numerical Simulation of Submicron Semiconductor Devices* (Artech House, Norwood, MA, 1993).